



Strong light-matter coupling in MoS₂

Patryk Kusch , Niclas S. Mueller , Martin T. Hartmann, and Stephanie Reich
Freie Universität Berlin, Department of Physics, Arnimallee 14, 14195 Berlin, Germany



(Received 12 March 2021; revised 21 May 2021; accepted 24 May 2021; published 7 June 2021)

Polariton-based devices require materials where light-matter coupling under ambient conditions exceeds losses, but our current selection of such materials is limited. Here we measured the dispersion of polaritons formed by the *A* and *B* excitons in thin MoS₂ slabs by imaging their optical near fields. We combined fully tunable laser excitation in the visible with a scattering near-field optical microscope to excite polaritons and image their optical near fields. We obtained the properties of bulk MoS₂ from fits to the slab dispersion. The in-plane excitons are in the strong regime of light-matter coupling with a coupling strength (40 – 100 meV) that exceeds their losses by at least a factor of two. The coupling becomes comparable to the exciton binding energy, which is known as very strong coupling. MoS₂ and other transition metal dichalcogenides are excellent materials for future polariton devices.

DOI: [10.1103/PhysRevB.103.235409](https://doi.org/10.1103/PhysRevB.103.235409)

I. INTRODUCTION

Exciton polaritons are mixed states of light and matter that form if the interaction strength between the exciton as a material excitation and the photons exceeds the losses in the material [1]. These quasiparticles are promising to transmit and convert information as they have long propagation length and mix the light and matter degrees of freedom. Polaritons have been studied profoundly in matter-filled photonic cavities and artificial nanoscale systems [1,2]. Observing them in three-dimensional (3D) materials, however, proved challenging, because the oscillator strengths of 3D excitons are often weak and their binding energies are smaller than the thermal energy at room temperature [3,4]. For example, the polariton coupling energy of the exciton in GaAs is $g = 7.8$ meV [4]. Measuring GaAs polaritons requires high-quality crystals and cryogenic temperatures. Similar values are found in many other bulk semiconductors [5]. A notable exception are wide band-gap semiconductors like ZnO and GaN, which makes them promising materials for polariton devices like ultralow threshold lasers [5–7]. The polariton coupling strength in, e.g., ZnO reaches 60 meV for the *A* and 140 meV for the *B* exciton that both have energies ≈ 3.31 eV (Ref. [6]). The high-exciton energies in ZnO and similar semiconductors, however, restrict such devices to the ultraviolet energy range. In addition, wide band-gap semiconductors have low dielectric constants limiting their ability to confine and guide light.

Transition metal dichalcogenides (TMDCs) are layered semiconductors with band gaps in the visible and near-infrared energy range. TMDCs have high-exciton binding energies (50–200 meV), a high-oscillator strength, and large dielectric constants [8–12]. They are covalently bound within the layers with a chemical composition MX₂, where M = Mo, W and X = S, Se [8]. The layers are held together by van der Waals forces, which allow to exfoliate TMDCs down to the limit of a single monolayer. TMDCs have two in-plane

polarized excitons, the *A* and *B* exciton that both arise from transitions at the *K* point of the Brillouin zone [8,11,13–15]. When the TMDCs are inserted into photonic cavities, these excitons form polaritons with cavity photons [9,10,15]. First studies of light-matter coupling in TMDCs focused on monolayers in metallic or dielectric cavities [10,16,17]. The polariton dispersion of an MoS₂ monolayer was measured by scanning the incident angle of the light in a cavity setup [16]. The system had two distinct polariton branches that were separated by a gap with the minimum energy $\Omega_r = 2g = 46$ meV (Rabi splitting). Attempts to similarly measure the dispersion in free-standing flakes (10 – 100 nm thickness) by reflectance were hindered by the broad spectral features and the large index of refraction that restricts the accessible propagation direction to be within 20° of the plane normal [9]. Estimates of the coupling strength from the dispersion around Γ gave values of 30 – 60 meV for the *A* and *B* exciton alike. Hu *et al.* [18] introduced scattering scanning near field optical microscopy (s-SNOM) to access the polariton dispersion of TMDCs in the near infrared. They imaged the dispersion of MoSe₂ around the energy of the *A* exciton (1.55 eV) and found $\Omega_r \approx 100$ meV. The light-matter coupling strength in monolayers and thin slabs of TMDCs ($g \approx 20 - 50$ meV) appears much higher than in classical semiconductors. The coupling strength in bulk TMDCs may be argued to be even larger, because only a fraction of the electromagnetic field overlaps with the material in thin samples [19].

The second parameter that controls the regime of strong light-matter coupling is the decay rate of the coupling states [1]. Specifically, strong light-matter coupling is reached if g is larger than the homogeneous broadening. Polariton formation and strong coupling appear robust against inhomogeneous broadening as long as the inhomogeneous broadening remains smaller than the Rabi splitting [20]. The typical exciton linewidths of TMDC monolayers (50 meV, Refs. [8,13,21,22]) are caused by inhomogeneous

broadening as shown exemplary for a WSe₂ monolayer where the homogeneous width of the *A* exciton at low temperatures (2 meV) was an order of magnitude smaller than its peak width (50 meV) [23,24]. The decay times of the *A* and *B* excitons at room temperature were measured and calculated as ≈ 1 ns (5 μ eV) in MoS₂ [25–27]. Reaching the regime of strong coupling in TMDCs appears within easy reach when considering the narrow intrinsic width of the exciton lines. On the other hand, the inhomogeneous broadening is strong and may prevent the observation of the effect. Given the uncertainties in coupling and damping rates, it remains open whether bulk TMDCs are materials with strong light-matter coupling under ambient conditions, i.e., if the coupling strength g exceeds their intrinsic damping rate γ .

Here we determine light-matter coupling in bulk MoS₂ from the polariton dispersion measured in thin slabs. We measured the polariton wavelength with a s-SNOM for various excitation wavelengths in the visible (700–540 nm). From the fits of the dispersion we obtained a coupling strength of 40 meV for the *A* exciton and 100 meV for the *B* exciton at room temperature. Both excitons in MoS₂ are in the strong coupling regime with similar coupling strength expected in other TMDCs. TMDCs are excellent materials to exploit polaritons under ambient conditions from 3D crystals down to 2D monolayers.

II. THEORY

Exciton polaritons are observed in bulk materials by their reflection, absorption, and luminescence spectra, but such experiments require highly pure samples [4,28]. Alternatively, propagating exciton-polariton modes may be imaged in thin slabs by SNOM as suggested by Hu *et al.* [18]. They used TMDC slabs that were thick enough to prevent quantum confinement of the exciton states, but thin enough to support waveguided photons [29,30]. Such measurements can be used to determine the polariton properties of the bulk material as we will show now.

To describe polariton formation in a thin TMDC slab, we first introduce the dielectric properties of a bulk exciton polariton and then consider the solutions for the waveguided modes. An exciton polariton forms through the interaction of an exciton ω_{ex} with a photon ω_{pt} . Inside the material the two independent (quasi)particles, photon and exciton, are replaced by the exciton-polariton as a new quasiparticle. The formation of the coupled state has some interesting consequences; for example, radiative decay is no longer a loss channel for the material excitation because the polariton continuously converts from a matter into a photonic excitation and vice versa [4]. We consider a layered material where the in-plane dielectric function $\varepsilon_i(\omega)$ is given by a background dielectric constant ε_b plus resonances by two excitons. Such an ansatz describes the contribution of the *A* and *B* exciton of MoS₂ to the optical properties of the material [4,11],

$$\begin{aligned} c^2 Q^2 &= \varepsilon_i(\omega) \omega^2 \\ &= \varepsilon_b \left(1 - \frac{4g_A^2}{\omega^2 - \omega_A^2 + i\gamma_A \omega} - \frac{4g_B^2}{\omega^2 - \omega_B^2 + i\gamma_B \omega} \right) \omega^2. \end{aligned} \quad (1)$$

Here ω_{ex} ($ex = A, B$) are the energies of the *A* and *B* exciton and γ_{ex} their damping constants. Q is the complex exciton-polariton wave vector. The out-of-plane dielectric function of the material $\varepsilon_o(\omega)$ is assumed to be constant.

Equation (1) connects two complex quantities, namely, frequency ω and wave vector Q , and requires a 4D plot for representation [31]. The standard way of visualizing the polariton dispersion is to impose real values for Q and plot the real part of the frequency $Re(\omega)$ versus $Re(Q)$. In this plot the polariton dispersion contains two branches with a minimum separation Ω_r^{ex} . These so-called upper and lower polariton branches are indeed observed in experiments, if the experimental setup imposes real values on the polariton wave vector, e.g., luminescence, light scattering, and reflection [9,32–34]. SNOM, in contrast, imposes real frequencies because the system is driven by a laser and exciton propagation and decay are observed in real space [18,31,35]. The $Re(\omega)$ over $Re(Q)$ dispersion then shows a backbending close to the resonance frequency. The Rabi splitting is found by the energetic difference between the lowest and the highest polariton energies at the crossing point between the dispersion of light and the exciton resonance energy [31,32].

We now consider electromagnetic waves in a thin slab of a material. In a slab with thickness d photons propagate as quantized waveguide eigenmodes ($d \ll \lambda_{pt}$, λ_{pt} vacuum photon wavelength). A free-standing slab in air supports a transverse electric (TE) and transverse magnetic (TM) waveguide mode down to vanishing slab thickness [29,30], but a minimum slab thickness is required to guide photons in an asymmetric dielectric environment like a flake on a substrate [30]. We are particularly interested in the thickness range around $d \approx 50$ nm where only the lowest-order TE₀ and TM₀ modes are allowed [29]. The dispersion of the TE₀ and TM₀ modes is described by effective dielectric functions that depend on the slab thickness and the dielectric properties of the slab and its surrounding [12,29]. The effective dielectric function for the TM₀ mode ε_{TM} is found from the condition [29]

$$\begin{aligned} \frac{2\pi d}{\lambda_{pt}} \sqrt{\varepsilon_i(1 - \varepsilon_{TM}/\varepsilon_o)} &= \tan^{-1} \left[\frac{\varepsilon_i \sqrt{\varepsilon_{TM} - 1}}{\sqrt{\varepsilon_i(1 - \varepsilon_{TM}/\varepsilon_o)}} \right] \\ &+ \tan^{-1} \left[\frac{\varepsilon_i \sqrt{\varepsilon_{TM} - \varepsilon_s}}{\varepsilon_s \sqrt{\varepsilon_i(1 - \varepsilon_{TM}/\varepsilon_o)}} \right]. \end{aligned} \quad (2)$$

λ_{pt} is the wavelength of light in vacuum and d the thickness of the slab. We assumed a flake in air on a substrate with ε_s ($\varepsilon_s = 2.1$ for SiO₂); ε_i is the dielectric function of the material for light polarized along the planes, see Eq. (1), and ε_o is the dielectric function for out-of-plane polarization. A similar condition yields the effective dielectric function for the TE₀ mode ε_{TE} [29]

$$\frac{2\pi d}{\lambda_{pt}} \sqrt{\varepsilon_i - \varepsilon_{TE}} = \tan^{-1} \left(\frac{\sqrt{\varepsilon_{TE} - 1}}{\sqrt{\varepsilon_i - \varepsilon_{TE}}} \right) + \tan^{-1} \left(\frac{\sqrt{\varepsilon_{TE} - \varepsilon_s}}{\sqrt{\varepsilon_i - \varepsilon_{TE}}} \right). \quad (3)$$

The characteristic dispersion of the TE₀ and TM₀ mode in slabs of layered material is shown in Fig. 1. Since the

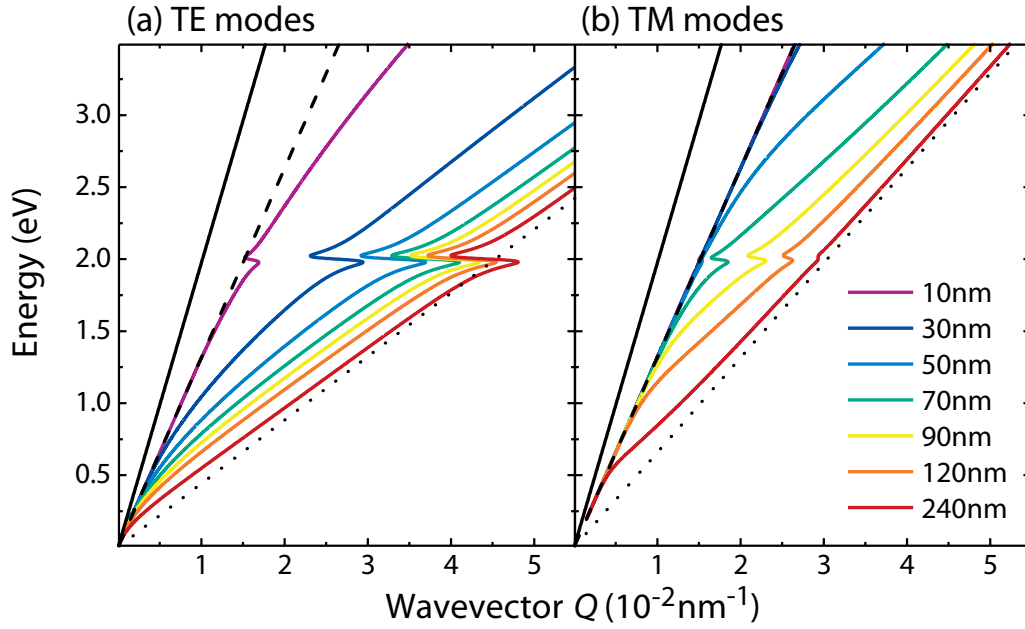


FIG. 1. Dispersion of the (a) TE₀ and (b) TM₀ modes in a thin slab of a layered material with an exciton resonance. The slab thickness is shown in the legend in (b). The full line is the photon dispersion in air, the dashed line is the dispersion of the substrate with $\epsilon_s = 2.25$, and the dotted line is the dispersion for a dielectric constant (a) $\epsilon_b = 20$ and (b) $\epsilon_o = 9$. The exciton was modeled as being polarized within the plane with $\omega_{ex} = 2$ eV, $\gamma_{ex} = 50$ meV, and $g_{ex} = 100$ meV.

dispersion of both modes contains features originating from the in-plane dielectric function, Eqs. (2) and (3), the TE or TM dispersion may be used to determine ϵ_i of the bulk material. The TE₀ mode exists already for very thin layers (10 nm); see the purple line in Fig. 1(a). The polariton-induced backbending is only weakly pronounced for thin slabs because of the limited overlap between the TE₀ mode and the slab material. The dispersion of this in-plane polarized mode rapidly converges to ϵ_i with increasing d ; see the red and dotted lines in Fig. 1. The TE₀ mode is independent of the out-of-plane dielectric function ϵ_o ; see Eq. (3). The situation is quite different for the TM₀ mode, where the electric field is predominantly oriented perpendicular to the layers, but also contains in-plane contributions. This mode requires a minimum thickness of $d = 50$ nm, light blue line in Fig. 1(b); for large d , it converges to ϵ_o , dotted line. Similar to the TE₀ mode, the backbending of the TM₀ mode is small for small d . The backbending increases with d , but exists only due to the in-plane component of the electric field, which vanishes for large d . The result is a maximum in the backbending for a thickness of 90 nm in Fig. 1(b) and a smaller Rabi splitting than for the TE₀ mode at any given thickness. In any case, fitting the TE or TM modes in thin slabs with Eqs. (2) and (3) yields the polariton dispersion or dielectric function of the underlying bulk material.

III. EXPERIMENTS

To measure the dispersion of the waveguided modes, we imaged their near fields on MoS₂ flakes using a s-SNOM (Ref. [37]) operating at excitation energies in the visible; see Fig 2. Polaritons manifest in near-field images through

interference between various scattering pathways in the SNOM. To obtain the dispersion, we repeated the experiment for various excitation wavelengths and determined the polariton wave vector as a function of energy. Such experiments have been reported only for infrared wavelengths or single-line laser excitation [12,18,29]. Here we implement it for visible excitation (up to 540 nm) using a fully tunable, narrow-line, and noise-suppressed laser.

Thin flakes of MoS₂ on a Si substrate with 300 nm SiO₂ were prepared by mechanical exfoliation. The substrate was sonicated (20–30 min), washed (isopropanol, acetone), and dried under nitrogen gas. We cleaved a piece of MoS₂ several times with Scotch tape and then transferred it to the freshly prepared substrate. We examined the size and thickness of the flakes by atomic force microscopy (AFM). The SNOM measurements were conducted on flakes of subwavelength thickness that are suitable as waveguides. In this paper we report the results obtained on a flakes with $d = 58, 68,$ and 82 nm.

In the s-SNOM (neasn timer by neaspec) the laser illuminates a metallic AFM tip; see Fig. 2(a). The tip produces an optical near field that excites slab polaritons in the flake. A mirror collects the light that gets scattered by the tip or emitted by the sample; see Fig. 2(b). The light is demodulated in a pseudoheterodyne detection setup (3rd harmonic) [38], which produces a near-field image of the sample, Fig. 2(c), with characteristic fringes and patterns that we will further analyze below. The AFM topography of the same area, Fig. 2(d), is completely flat and featureless. The microscopy images were produced simultaneously using enhanced platinum tips (neaspec) working in tapping mode at the tip eigenfrequency ≈ 350 kHz with an amplitude of 50 nm. A unique feature of

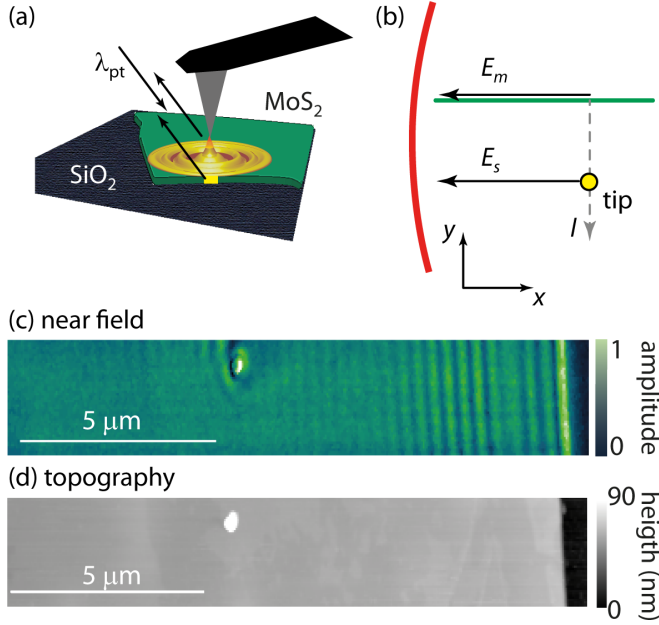


FIG. 2. Near-field imaging. (a) Sketch of the metallic tip that excites an exciton polariton in a flake of MoS₂ (green) when illuminated by a laser with wavelength λ_{pt} . The polariton scatters at the edge of the sample and is emitted partly into free space. Light gets scattered also by the tip directly, which will interfere with the edge-emitted photons. (b) On-top view of light emission in the $\theta = 0^\circ$ configuration. θ is the angle between the optical axis of the mirror and the sample edge, see supplemental material for details [36]. The electric fields E_s produced at the tip and E_m produced at the edge interfere in the detection system (indicated as the red line representing the collecting mirror). Yellow dot: tip, green line: MoS₂ edge. The inset at the bottom shows the in-plane coordinate system. (c) Near-field amplitude on an MoS₂ flake with $d = 68$ nm excited at $\lambda_{pt} = 578$ nm. Clearly visible are the interference patterns from the superposition of E_s and E_m . (d) Topography image recorded simultaneously with (c).

our s-SNOM system is the wide range of laser wavelengths in the visible 700–450 nm (1.77–2.75 eV) that are provided by the fully tunable C-Wave laser (Hübner Photonics). Similar near-field images as in Fig. 2 were obtained for the energy range 1.79–2.3 eV, which covers the A and B exciton resonance of MoS₂.

There are several mechanisms that can give rise to the interference patterns in Fig. 2(c). The dominant interference mechanism when exciting TMDCs in the visible is that edge-emitted light with electric field amplitude E_m interferes with light that was scattered directly by the metallic tip E_s ; see Fig. 2(b) [18,35]. We worked in a configuration where the emissive edge is parallel to the optical axis of the collecting mirror as sketched in the top view in Fig. 2 b ($\theta = 0^\circ$; see supplemental material [36]). We chose this configuration because it is free of systematic errors that arise from the limited knowledge of the exact alignment configuration [18]. A near-field image as shown in Fig. 3(c) shows the field amplitude of the tip and edge-emitted waves $A_{nr} \propto |E_s + E_m|$. In the $\theta = 0^\circ$ configuration and for a tip position at a point l along a line perpendicular to the edge, A_{nr} at the detector is given by, see

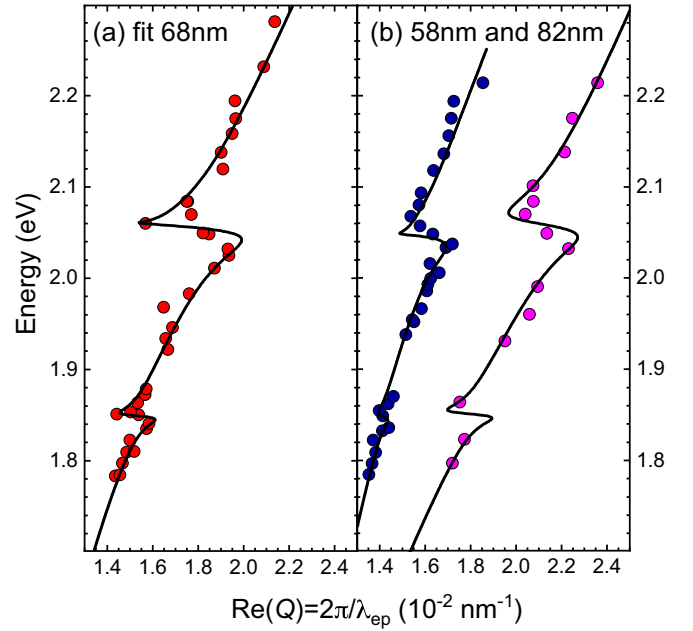


FIG. 3. Experimental dielectric function of thin MoS₂ slabs. Dots: Dispersion of the TM₀ mode measured with the s-SNOM at a flake with (a) $d = 68$ nm, (b) 58 nm (blue), and 82 nm (purple). (a) The line is a fit to the experimental data with Eq. (2). (b) The lines are plots of the predicted TM₀ dispersion using the fit parameters of (a); see Table I.

supplemental material [36],

$$A_{nr}(l) \propto |E_s + E_m| = \sqrt{A_s^2 + A_m^2 e^{-2\gamma_0 l} + 2A_s A_m e^{-\gamma_0 l} \cos \frac{2\pi}{\lambda_{ep}} l}, \quad (4)$$

with

$$E_s = A_s e^{i(k_x x + \omega t)} \quad (5)$$

and

$$E_m = A_m e^{iQl} e^{i(k_x x + \omega t)}. \quad (6)$$

A_s is the amplitude of the light scattered by the tip and A_m is the amplitude of the light emitted at the edge toward the collecting mirror. Q is the complex wave vector of the exciton polariton propagating along the y direction; see Fig. 2(b) for the coordinate system. Its real part $\text{Re}(Q) = 2\pi/\lambda_{ep}$ yields the polariton wavelength λ_{ep} ; its imaginary part $\text{Im}(Q) = \gamma_Q$ is the damping of the polariton; k_x is the x component of the photon in free space.

TABLE I. Fit parameters of the MoS₂ excitons. ω_{ex}^{LT} is the splitting of the transverse and longitudinal exciton related to the Rabi splitting by $\Omega_r^{ex} = \sqrt{2\omega_{ex}^{LT}\omega_{ex}}$.

	ω_{ex} (eV)	γ_{ex} (meV)	Ω_r (meV)	g (meV)	ω_{ex}^{LT} (meV)
A exciton	1.850	11	84	42	1.6
B exciton	2.053	35	194	97	9.4

We extracted line scans perpendicular to the sample edge from the near-field images as in Fig. 2(c). The fit with Eq. (4) yields the wavelength and damping of the polariton. Equation (4) is valid only for $\theta = 0^\circ$ as in Fig. 2(b). The fringe period, i.e., the distance between two interference maxima, deviates rapidly from λ_{ep} for any misalignment. We carefully verified the dependence and corrected the measured λ_{ep} for the misalignment; see supplemental material for details [36].

IV. RESULTS

The experimental dispersion of MoS₂ flakes with thicknesses below 100 nm shows two backbending slopes around 1.85 and 2.05 eV; see Fig. 3. The backbending is weakest for the thinnest flake with $d = 58$ nm. It increases for 68 nm and then again gets weaker for the thickest 82-nm flake. The increase and decrease of the backbending is characteristic of the TM₀ mode; see Fig. 1. We detected no signatures of the TE₀ mode in our near-field images. This is reasonable because the predominantly z polarized near field of the metallic tip cannot couple to TE eigenmodes that are polarized in plane. The line in Fig. 3(a) is a fit to the experimental data obtained at the $d = 68$ nm flake with Eq. (2). We used the same parameters, Table I, to calculate the dispersion for $d = 58$ and 82 nm. The fit describes the data obtained in the other two flakes very well; see Fig. 3(b). In particular, it reproduces the decreasing Rabi splitting for smaller and larger thicknesses.

The pronounced backbending of the TM₀ dielectric function implies that the A and B excitons of the MoS₂ slabs are in the regime of strong light-matter coupling [1,31]. More importantly, the coupling remains strong between excitons in bulk MoS₂ and free-space photons; see Table I. We find a coupling strength $g_A = \Omega_c^A/2 = 42$ meV for the A exciton in bulk MoS₂ that is four times larger than its damping $\gamma_A = 11$ meV. The coupling strength of the B exciton $g_B = 97$ meV exceeds its decay rate $\gamma_B = 35$ meV almost by a factor of three. The Rabi splitting in MoS₂ is an order of magnitude larger than in classical semiconductors like GaAs. It rivals the coupling found in wide band-gap semiconductors with low dielectric constants [5], but the dielectric constants of MoS₂ are large. We find an out-of-plane constant $\epsilon_o = 7.6$ and an in-plane background dielectric constant $\epsilon_b = 25$, in good agreement with previous measurements [12,29]. At the same time, the exciton energies $\omega_A = 1.85$ eV and $\omega_B = 2.05$ eV make MoS₂ an attractive material for polariton-based devices at visible and near-infrared wavelengths [5].

Interestingly, the exciton polaritons of MoS₂ also fulfill the condition for very strong light-matter coupling. Very strong coupling means that the coupling strength is comparable to the exciton binding energy E_{ex}^b , i.e., $\beta_{ex} = g/E_{ex}^b \approx 1$ [39]. To calculate β we need the exciton binding energies of bulk MoS₂ that, surprisingly, remain debated [11,14,21]. Depending on the interpretation of the optical spectra $E_A^b = 40 - 80$ meV and $E_B^b = 100 - 130$ meV placing $\beta_A \approx 0.6 - 1.25$ and $\beta_B \approx 0.8 - 1$. For β approaching one, light-matter coupling contributes to the interaction between the electron and the hole forming the exciton [39]. They start to interact by emitting and absorbing virtual photons, which reduces the exciton radius in the lower and increases the radius in the upper polariton state. The condition for very strong coupling is only met by

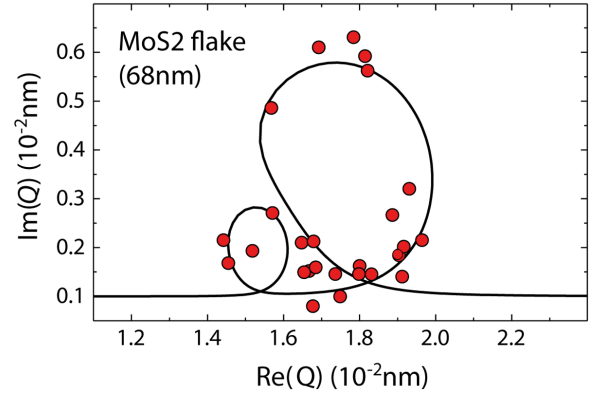


FIG. 4. Imaginary and real parts of the polariton wave vector in the $d = 68$ nm MoS₂ flake. The data points were obtained from the near-field images; see Supplemental Fig. S1. The line is a fit obtained from the data in Fig. 3(a); see text.

bulk MoS₂ and lost for thin slabs and monolayers because the coupling decreases to $g \approx 20$ meV (Ref. [16]) and the binding energy increases to $E_b \gtrsim 200$ meV (Refs. [8,40]) so that β drops to 0.1 or less.

The damping rates γ_A and γ_B extracted from the fits to the TM₀ dispersion are smaller than the inhomogeneous linewidth of MoS₂ flakes at room temperature [8,13]. Nevertheless, they most likely underestimate the lifetime of the MoS₂ excitons because we neglected the damping of the photonic mode via edge emission. γ_B is three times larger than γ_A , which agrees with the range of rates observed for the two excitonic states [27,41]. We can also determine the spatial damping of the MoS₂ polaritons from the near-field images because the interference patterns exist over several micrometers; see Fig. 2(c). The damping depends strongly on the exciting laser frequency: While the pattern extends for some micrometers for frequencies away from the A and B exciton, Supplemental Fig. S1 [36], it drops to hundreds of nanometers for resonant excitation. We extract the spatial damping from the fits with Eq. (4). A plot of the imaginary versus the real part of the wave vector Q in Fig. 4 shows two loops at the wave vector of the excitons in the uncoupled system. The looping shape is another signature of strong coupling in photonic systems confirming the result of the $Re(\omega)$ versus $Re(Q)$ plot in Fig. 3 [31]. We calculated the full line in Fig. 4 using Eq. (2) with the fitting parameters obtained from the polariton dispersion and adding a constant damping of 10^{-3} nm^{-1} . The latter represents scattering by crystal imperfections and errors introduced by the experimental setup. With increasing distance between tip and edge the edge-emitted photons propagate off the optical axis, which eventually reduces the interference amplitude. The maximum propagation length $l_p = 1/2\text{Im}(Q)$ of $5 \mu\text{m}$ in Fig. 4, therefore, poses a lower bound to the polariton propagation. In resonance with the B exciton the propagation length drops to 100 nm, but even this value is longer than for the bulk polariton. Using the parameters of Table I we predict a minimum propagation length ≈ 20 nm for polaritons at the exciton energies in the bulk. This high damping is a consequence of the strong coupling because these polariton frequencies correspond to the forbidden gap that opens

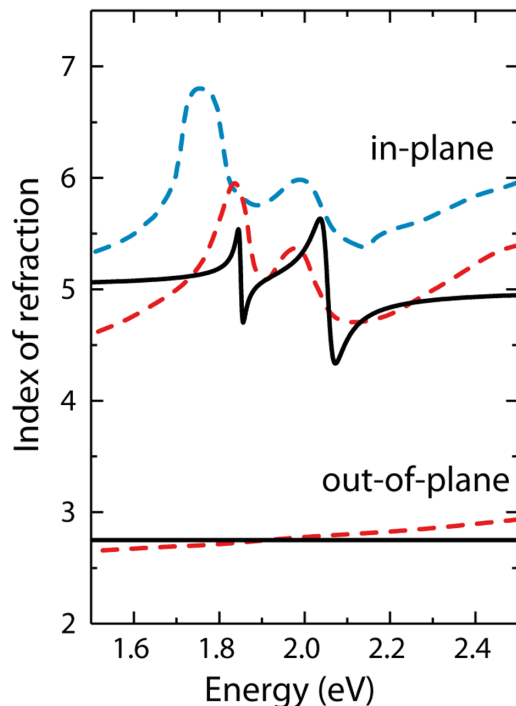


FIG. 5. Index of refraction in MoS₂. The full line shows the polaritonic contribution to the index of refraction as determined from the slab measurements. The dashed red line is for ellipsometry measurements (Ref. [12]) and the dashed blue line is from optical reflectance (Ref. [11]).

between lower and upper polaritons in the dispersion for real Q vectors [4,31].

It is instructive to deduce the polariton contribution to the bulk dielectric function in MoS₂ from our slab measurements. Figure 5 shows the polaritonic part of the index of refraction compared to reflectance (blue) and ellipsometric (red) measurements on bulk MoS₂ [11,12]. The overall agreement is quite remarkable confirming that the optical response of MoS₂ in the visible is dominated by exciton-related effects. The

bulk measurements are much broader in line width than the polaritonic part of the index of refraction. This is due to band-to-band transitions and defect-related excitations. It would be interesting to obtain more experimental data at low temperatures to better distinguish between intrinsic and extrinsic sources of damping. The similarity between the polaritonic contribution to the index of refraction obtained from the slabs and the experiments on bulk MoS₂ shows that polaritons need to be considered in the description of this material. We note that the refractive indices in Fig. 5 are strongly anisotropic with a difference $\Delta n_{oi} \approx 2$ between the in-plane and out-of-plane refractive index [11,12]. Polaritons can be guided and confined efficiently along the MoS₂ layers even in the bulk material.

V. CONCLUSION

In conclusion, we measured the dispersion of the transverse magnetic modes in slabs of MoS₂ using near-field optical microscopy with fully tunable visible excitation. We determined the strength of light-matter coupling in bulk MoS₂ from the dispersion of the slab mode. The A and B excitons are in the regime of strong light-matter coupling with a coupling strength of 40 meV for the A and 100 meV for the B excitons, which exceeds their losses by more than a factor of two. Because their coupling strength is also comparable to the exciton binding energy, the formation of the exciton and its properties depend also on the coupling to light. MoS₂ combines strong light-matter coupling with a large index of refraction and a strong anisotropy in its dielectric response. It is a very promising material for polariton-based devices operating under ambient conditions.

ACKNOWLEDGMENTS

We acknowledge financial support by the European Research Council (ERC) under Grant DarkSERS (772108) and by the German Science Foundation (DFG) within the Priority Program SPP 2244 “2DMP”

- [1] D. G. Baranov, M. Wersäll, J. Cuadra, T. J. Antosiewicz, and T. Shegai, Novel nanostructures and materials for strong light-matter interactions, *ACS Photon.* **5**, 24 (2018).
- [2] A. Frisk Kockum, A. Miranowicz, S. De Liberato, S. Savasta, and F. Nori, Ultrastrong coupling between light and matter, *Nat. Rev. Phys.* **1**, 19 (2019).
- [3] P. Yu and M. Cardona, *Fundamentals of Semiconductor Physics* (Springer, Heidelberg, 1996).
- [4] L. C. Adreani, Optical transitions, excitons, and polaritons in bulk and low-dimensional semiconductor structures, in *Confined Electrons and Photons*, edited by E. Burstein and C. Weisbuch (Plenum Press, New York, 1995), p. 57.
- [5] D. Sanvitto and S. Kéna-Cohen, The road towards polaritonic devices, *Nat. Mat.* **15**, 1061 (2016).
- [6] L. Sun, Z. Chen, Q. Ren, K. Yu, L. Bai, W. Zhou, H. Xiong, Z. Q. Zhu, and X. Shen, Direct Observation of Whispering

- Gallery Mode Polaritons and Their Dispersion in a ZnO Tapered Microcavity, *Phys. Rev. Lett.* **100**, 156403 (2008).
- [7] J.-W. Kang, B. Song, W. Liu, S.-J. Park, R. Agarwal, and C.-H. Cho, Room temperature polariton lasing in quantum-heterostructure nanocavities, *Sci. Adv.* **5**, eaau9338 (2019).
- [8] G. Wang, A. Chernikov, M. M. Glazov, T. F. Heinz, X. Marie, T. Amand, and B. Urbaszek, Excitons in atomically thin transition metal dichalcogenides, *Rev. Mod. Phys.* **90**, 021001 (2018).
- [9] B. Munkhbat, D. G. Baranov, M. Stührenber, M. Wersall, A. Bisht, and T. Shegai, Self-hybridized exciton polaritons in multilayers of transition metal dichalcogenides for efficient light absorption, *ACS Photon.* **6**, 139 (2019).
- [10] F. Hu and Z. Fei, Recent progress on exciton polaritons in layered transition-metal dichalcogenides, *Adv. Opt. Mater.* **8**, 1901003 (2019).

- [11] R. A. Neville and B. L. Evans, The band edge excitons in 2H-MoS₂, *Phys. Status Solidi B* **73**, 597 (1976).
- [12] G. A. Ermolaev, D. V. Grudin, Y. V. Stebunov, K. V. Voronin, V. G. Kravets, J. Duan, A. B. Mazitov, G. I. Tselikov, A. Bylinkin, D. I. Yakubovskiy, S. M. Novikov, D. G. Baranov, A. Y. Nikitin, I. A. Kruglov, T. Shegai, P. Alonso-Gonzalez, A. N. Grigorenko, A. V. Arsenin, K. S. Novoselov, and V. S. Volkov, Giant optical anisotropy in transition metal dichalcogenides for next-generation photonics, *Nat. Commun.* **12**, 854 (2021).
- [13] K. F. Mak, C. Lee, J. Hone, J. Shan, and T. F. Heinz, Atomically Thin MoS₂: A New Direct-Gap Semiconductor, *Phys. Rev. Lett.* **105**, 136805 (2010).
- [14] E. Fortin and F. Raga, Excitons in molybdenum disulphide, *Phys. Rev. B* **11**, 905 (1975).
- [15] C. Schneider, M. M. Glazov, T. Korn, S. Höfling, and B. Urbaszek, Two-dimensional semiconductors in the regime of strong light-matter coupling, *Nat. Commun.* **9**, 2695 (2018).
- [16] X. Liu, T. Galfsky, Z. Sun, F. Xia, E. chen Lin, Y.-H. Lee, S. Kena-Cohen, and V. M. Menon, Strong light-matter coupling in two-dimensional atomic crystals, *Nat. Photon.* **9**, 30 (2014).
- [17] L. C. Flatten, Z. He, D. M. Coles, A. A. P. Trichet, A. W. Powell, R. A. Taylor, J. H. Warner, and J. M. Smith, Room-temperature exciton-polaritons with two-dimensional WS₂, *Sci. Rep.* **6**, 33134 (2016).
- [18] F. Hu, Y. Luan, M. E. Scott, J. Yan, D. G. Mandrus, X. Xu, and Z. Fei, Imaging exciton-polariton transport in MoSe₂ waveguides, *Nat. Photon.* **11**, 356 (2017).
- [19] V. Savona, L. C. Andreani, P. Schwendimann, and A. Quattropani, Quantum well excitons in semiconductor microcavities: Unified treatment of weak and strong coupling regimes, *Sol. Stat. Commun.* **93**, 733 (1995).
- [20] J.-M. Manceau, G. Biasiol, N. L. Tran, I. Carusotto, and R. Colombelli, Immunity of intersubband polaritons to inhomogeneous broadening, *Phys. Rev. B* **96**, 235301 (2017).
- [21] N. Saigal, V. Sugunakar, and S. Ghosh, Exciton binding energy in bulk MoS₂: A reassessment, *Appl. Phys. Lett.* **108**, 132105 (2016).
- [22] B. R. Carvalho, L. M. Malard, J. M. Alves, C. Fantini, and M. A. Pimenta, Symmetry-dependent exciton-phonon coupling in 2D and bulk MoS₂ Observed by Resonance Raman Scattering, *Phys. Rev. Lett.* **114**, 136403 (2015).
- [23] G. Moody, C. K. Dass, K. Hao, C.-H. Chen, L.-J. Li, A. Singh, K. Tran, G. Clark, X. Xu, G. Berghäuser, E. Malic, A. Knorr, and X. Li, Intrinsic homogeneous linewidth and broadening mechanisms of excitons in monolayer transition metal dichalcogenides, *Nat. Commun.* **6**, 8315 (2015).
- [24] F. Cadiz, E. Courtade, C. Robert, G. Wang, Y. Shen, H. Cai, T. Taniguchi, K. Watanabe, H. Carrere, D. Lagarde, M. Manca, T. Amand, P. Renucci, S. Tongay, X. Marie, and B. Urbaszek, Excitonic Linewidth Approaching the Homogeneous Limit in MoS₂-Based van der Waals Heterostructures, *Phys. Rev. X* **7**, 021026 (2017).
- [25] H. Shi, R. Yan, S. Bertolazzi, J. Brivio, B. Gao, A. Kis, D. Jena, H. G. Xing, and L. Huang, Exciton dynamics in suspended monolayer and few-layer MoS₂ 2D crystals, *ACS Nano* **7**, 1072 (2013).
- [26] M. Palummo, M. Bernardi, and J. C. Grossman, Exciton radiative lifetimes in two-dimensional transition metal dichalcogenides, *Nano Lett.* **15**, 2794 (2015).
- [27] T. Wang, Y. Zhang, Y. Liu, J. Li, D. Liu, J. Luo, and K. Ge, Layer-number-dependent exciton recombination behaviors of MoS₂ determined by fluorescence-lifetime imaging microscopy, *J. Phys. Chem. C* **122**, 18651 (2018).
- [28] D. D. Sell, S. E. Stokowski, R. Dingle, and J. V. DiLorenzo, Polariton reflectance and photoluminescence in high-purity GaAs, *Phys. Rev. B* **7**, 4568 (1973).
- [29] D. Hu, X. Yang, C. Li, R. Liu, Z. Yao, H. Hu, S. N. G. Coder, J. Chen, Z. Sun, M. Liu, and Q. Dai, Probing optical anisotropy of nanometer-thin van der Waals microcrystals by near-field imaging, *Nat. Commun.* **8**, 1471 (2017).
- [30] J. B. Khurgin, Two-dimensional exciton-polariton-light guiding by transition metal dichalcogenide monolayers, *Optica* **2**, 740 (2015).
- [31] C. Wolff, K. Busch, and N. A. Mortensen, Modal expansions in periodic photonic systems with material loss and dispersion, *Phys. Rev. B* **97**, 104203 (2018).
- [32] E. T. Arakawa, M. W. Williams, R. N. Hamm, and R. H. Ritchie, Effect of Damping on Surface Plasmon Dispersion, *Phys. Rev. Lett.* **31**, 1127 (1973).
- [33] C. H. Henry and J. J. Hopfield, Raman Scattering by Polaritons, *Phys. Rev. Lett.* **15**, 964 (1965).
- [34] N. S. Mueller, Y. Okamura, B. G. M. Vieira, S. Juergensen, H. Lange, E. B. Barros, F. Schulz, and S. Reich, Deep strong light-matter coupling in plasmonic nanoparticle crystals, *Nature (London)* **583**, 780 (2020).
- [35] Z. Fei, M. E. Scott, D. J. Gosztola, J. J. Foley, J. Yan, D. G. Mandrus, H. Wen, P. Zhou, D. W. Zhang, Y. Sun, J. R. Guest, S. K. Gray, W. Bao, G. P. Wiederrecht, and X. Xu, Nano-optical imaging of WSe₂ waveguide modes revealing light-exciton interactions, *Phys. Rev. B* **94**, 081402(R) (2016).
- [36] See supplemental material at <http://link.aps.org/supplemental/10.1103/PhysRevB.103.235409> for experimental details and additional data and modelings.
- [37] T. Taubner, R. Hillenbrand, and F. Keilmann, Performance of visible and mid-infrared scattering-type near-field optical microscopes, *J. Microsc.* **210**, 311 (2003).
- [38] R. Hillenbrand, B. Knoll, and F. Keilmann, Pure optical contrast in scattering-type scanning near-field microscopy, *J. Microsc.* **202**, 77 (2001).
- [39] J. B. Khurgin, Excitonic radius in the cavity polariton in the regime of very strong coupling, *Sol. Stat. Commun.* **117**, 307 (2001).
- [40] C. Zhang, A. Johnson, C.-L. Hsu, L.-J. Li, and C.-K. Shih, Direct imaging of band profile in single layer MoS₂ on graphite: Quasiparticle energy gap, metallic edge states, and edge band bending, *Nano Lett.* **14**, 2443 (2014).
- [41] S. Cha, J. H. Sung, S. Sim, J. Park, H. Heo, M.-H. Jo, and H. Choi, 1s-intraexcitonic dynamics in monolayer MoS₂ probed by ultrafast mid-infrared spectroscopy, *Nat. Commun.* **7**, 10768 (2016).